ICES Journal of Marine Science, 2022, **79**, 1312–1326
DOI: 10.1093/icesjms/fsac055
Advance access publication date: 13 April 2022
Original Article

ICES CIEM International Council for the Exploration of the Sea
Conseil International pour l'Exploration de la Mer

Spatiotemporal variability of euphausiids in the California Current Ecosystem: insights from a recently developed time series

Elizabeth M. Phillips [1,*], Dezhang Chu [1], Stéphane Gauthier [2,3], Sandra L. Parker-Stetter [4], Andrew O. Shelton [5] and Rebecca E. Thomas [1]

[1]Fishery Resource Analysis and Monitoring Division, Northwest Fisheries Science Center, National Marine Fisheries Service, National Oceanic and Atmospheric Administration, 2725 Montlake Blvd E, Seattle, WA 98112, USA
[2]Institute of Ocean Sciences, Fisheries and Oceans Canada, Sidney, BC V8L 5T5, Canada
[3]Department of Biology, University of Victoria, Victoria, BC V8P 5C2, Canada
[4]Resource Assessment and Conservation Engineering Division, Alaska Fisheries Science Center, National Marine Fisheries Service, National Oceanic and Atmospheric Administration, 7600 Sand Point Way NE, Seattle, WA 98115, USA
[5]Conservation Biology Division, Northwest Fisheries Science Center, National Marine Fisheries Service, National Oceanic and Atmospheric Administration, 2725 Montlake Blvd E., Seattle, WA 98112, USA

[*] *Corresponding author: tel: 1-425-666-9967; e-mail:* elizabeth.phillips@noaa.gov.

Euphausiids, or krill, are important energy links between primary producers and higher trophic levels in the California Current Ecosystem (CCE), but a thorough understanding of their variability at the coast-wide scale is limited. Using fisheries acoustics data collected during biennial joint US–Canada Integrated Ecosystem and Acoustic Trawl Surveys for Pacific hake (*Merluccius productus*), we developed a time series ($n = 8$ years; 2007–2019 odd years inclusive, and 2012) of krill abundance and examined relationships with environmental factors. Krill were located in waters off the west coasts of the United States and Canada, primarily in shallow basins and on the continental shelf, with greatest kernel density estimates near Cape Mendocino and the Juan de Fuca eddy system. Coast-wide krill abundance was variable, and lowest in 2015 during an extended marine heat wave, when 91% were located in British Columbia. Using hierarchical generalized additive models, we predicted greatest krill abundance in cooler waters (0.2°C below the time series average), within 10–20 km of the shelf break, and in bottom depths between 200 and 400 m. This newly developed coast-wide time series of krill abundance and distribution will inform ecosystem-based fisheries management efforts, and offers additional opportunities for studies of krill-dependent fish, seabirds, and marine mammals.

Keywords: *Euphausia pacifica*, fisheries acoustics, frequency differencing, krill, *Merluccius productus*, Pacific hake, *Thysanoessa spinifera*.

Introduction

Zooplankton are an important energy link between phytoplankton and higher trophic levels throughout the world's oceans (Richardson, 2008). In the northeast Pacific Ocean, euphausiids (Euphausiacea), or krill, are key zooplankton prey for a range of fish, seabirds, and marine mammals (Mauchline and Fisher, 1969). The highly productive California Current Ecosystem (CCE) supports a number of krill populations (Brinton, 1962), which in turn sustain important fishery resources including Pacific hake, *Merluccius productus* (Livingston, 1983) and Pacific salmon, *Oncorhynchus* spp (Peterson *et al.*, 1982). Krill in the CCE are also important prey for other predators such as Cassin's auklets, *Ptychoramphus aleuticus*, and blue whales, *Balaenoptera musculus* (Croll *et al.*, 1998; Sydeman *et al.*, 2006). Research on krill in the CCE has led to important insights on relationships between abundance, distribution, and dynamic ocean conditions (Mackas *et al.*, 2001; Santora *et al.*, 2011). However, a lack of broad-scale and spatially comprehensive data has prevented a full understanding of coast-wide patterns in krill distribution and variability in abundance, and analyses of the potential effects on dependent fish, seabirds, and marine mammals.

Krill abundance in the CCE increases seasonally in response to local primary production, which peaks in spring and summer (Mackas, 1992). This time period is typically characterized by intense wind-driven upwelling, which brings cold, nutrient-rich waters to the surface that generate large phytoplankton blooms and are positively correlated with increased krill abundance (Ressler *et al.*, 2005; Checkley and Barth, 2009). Dense krill aggregations are related to the location of bathymetric features including the continental shelf break and submarine canyons, where primary productivity is often enhanced (Mackas, 1992; Peterson *et al.*, 2000; Santora *et al.*, 2018). Krill often occur in patchily distributed aggregations, which result from the interaction of horizontal transport downstream of upwelling centers and a behavioural response of zooplankton to swim downwards against vertical currents (Mackas *et al.*, 1985, 1997; Genin, 2004). Mesoscale circulation patterns then maintain krill aggregations by increasing the residence time of upwelled water and prolonging primary production, allowing for extended grazing periods (Ressler *et al.*, 2005).

Basin-scale interannual and decadal temperature fluctuations also influence krill populations. The abundance of the most dominant and broadly ranging krill species in the CCE, *Euphausia pacifica*, is correlated to cool ocean conditions dominated by strong upwelling and sustained primary production (Brinton, 1962). Increases in water temperature

Received: November 5, 2021. **Revised:** February 22, 2022. **Accepted:** February 23, 2022

and decreases in primary production related to El Niño–Southern Oscillation (ENSO) events can reduce the overall abundance of *E. pacifica*, as well as neritic, cold-water *Thysanoessa spinifera* that co-occur with *E. pacifica* (Brinton and Townsend, 2003; Cimino *et al.*, 2020). ENSO events also alter the species composition of krill in the CCE by increasing poleward transport, resulting in greater abundances of warm-water krill species and fewer cold-water species (Marinovic *et al.*, 2002). A recent marine heat wave during 2014–2016 increased surface ocean water temperatures (Di Lorenzo and Mantua, 2016) and reduced the overall abundance of cold-water krill species in parts of the CCE (Peterson *et al.*, 2017; Lavaniegos *et al.*, 2019). Warmer waters associated with the marine heat wave also negatively impacted growth rates of *E. pacifica* and overall adult size (Robertson and Bjorkstedt, 2020), indicating that temperature plays an important role in the overall abundance and growth of krill in the CCE.

Krill abundance and distribution are often quantified using fisheries acoustics surveys because continuous, high-resolution horizontal and vertical data can be used to examine krill aggregations at a range of spatial scales. Acoustic surveys have successfully assessed krill populations in the Southern Ocean (Hewitt *et al.*, 2003), northern Atlantic Ocean (Everson *et al.*, 2007; McQuinn *et al.*, 2015), and eastern Pacific Ocean (Swartzman and Hickey, 2003). In the CCE, a number of studies using acoustic data collected at smaller geographic scales have linked krill abundance and distribution to environmental conditions (Ressler *et al.*, 2005; Santora *et al.*, 2011). However, systematically collected acoustic data throughout the full extent of the CCE has not been previously available to analyze coast-wide patterns of krill abundance and distribution.

The goal of this study was to process archived acoustic data collected during biennial joint US–Canada Integrated Ecosystem and Acoustic Trawl Surveys for Pacific hake to develop a time series of krill abundance and distribution in the CCE. We identified krill in the acoustic backscatter and quantified spatiotemporal variability in abundance between 2007 and 2019, in a survey area of approximately 221 000 km^2 from southern California, United States, to northern British Columbia, Canada. We also estimated relationships to bathymetric habitat features and dynamic environmental conditions including primary production and temperature to develop a better understanding of krill variability in the CCE to inform ecosystem-based management.

Material and methods

Survey area and study design

We used data from the National Oceanic and Atmospheric Administration Northwest Fisheries Science Center (hereafter, NOAA) and Fisheries and Oceans Canada (hereafter, DFO), which have conducted biennial joint US–Canada Integrated Ecosystem and Acoustic Trawl Surveys for Pacific hake along the west coasts of the United States and Canada since 2003. The biennial surveys were conducted during the summer months (June–September) when hake occurred in feeding aggregations near the continental shelf break. All surveys began in the south near Point Conception, California, United States (34.5°N), and moved north through British Columbia, Canada to Dixon Entrance, Alaska, United States (54.4°N). Each transect line crossed between the 50 m isobath and the 1500 m isobath, which allowed for data collection across continental shelf, shelf break, and slope habitat. Transects were generally oriented in an east–west direction along the coast except near Dixon Entrance, where they were oriented north–south (Figure 1). Transects were spaced approximately 16 or 32 km (10 or 20 nmi) apart, and the southern and northern extents, and to a lesser degree offshore extent, were determined by observed hake distribution (Fleischer *et al.*, 2008). The number of total transects surveyed varied annually, but typically ranged between 110 and 150 in total (Table 1). We used echosounder data from eight surveys between 2007 and 2019 (odd years inclusive, plus 2012) that included at least 38 and 120 kHz data that could be used to identify krill.

Acoustic data collection and processing

Downward-looking Simrad EK60 narrow-band, split-beam echosounders were used to collect acoustic data at multiple frequencies (18, 38, 70, 120, and/or 200 kHz) from multiple research vessels (Table 1). Depending on the vessel configuration and other survey needs, not all acoustic frequencies were available during each year; the 38 and 120 kHz data were common among all years. Acoustic data were recorded continuously from the sea surface to a depth of 750 m during daylight hours (i.e. from local sunrise to sunset, approximately 15 h per day). The normal ship survey speed was 5.1 m s^{-1} (10 knots) and data were collected using a 1.024-ms narrow-band pulse at a ping rate of 1 ping s^{-1}. All echosounders were calibrated prior to and/or after each survey using standard sphere methods (Demer *et al.*, 2015).

On-transect acoustic data were processed using Echoview version 9.0 (Echoview Pty Ltd, Hobart, Australia). Noise spikes were removed from all files using Echoview's impulse noise removal operator, and false bottoms were visually identified in the echogram and manually removed. Seafloor echoes were detected acoustically, inspected, and manually corrected as needed. Background noise was estimated based on the theory from De Robertis and Higginbottom (2007) using mean volume backscattering strength (S_v or MVBS, dB re 1 m^{-1}) measured in 40 ping × 10 m cells, and removed by subtracting the estimated background noise value from the original S_v values, using a maximum noise threshold of −125 dB and a signal-to-noise ratio filter with a threshold of 10 dB. Samples that did not pass this filter were classed as empty water, followed by smoothing of all cells to 5 pings × 5 samples. To account for variation in transducer depth on each vessel, the near-field range of the 38 kHz echosounder, surface noise intrusion, and to remove scattering from non-adult krill and other targets near the surface, data from within 50 m of the water surface were excluded from analyses. To account for decreasing signal-to-noise ratio with depth, particularly for the 120 kHz echosounder, data below a depth of 300 m were also excluded. In areas where the seafloor was shallower than 300 m, data from within 1 m of the seafloor were removed to avoid possible bottom echo intrusion. A small amount of krill backscatter very close to the seafloor may have been omitted due to this processing step, but we believed it to be negligible. The described distribution of adult krill during the day generally encompasses 100–250 m (Mackas *et al.*, 1997), so we assumed that the majority of krill present in the water column were detected using these methods.

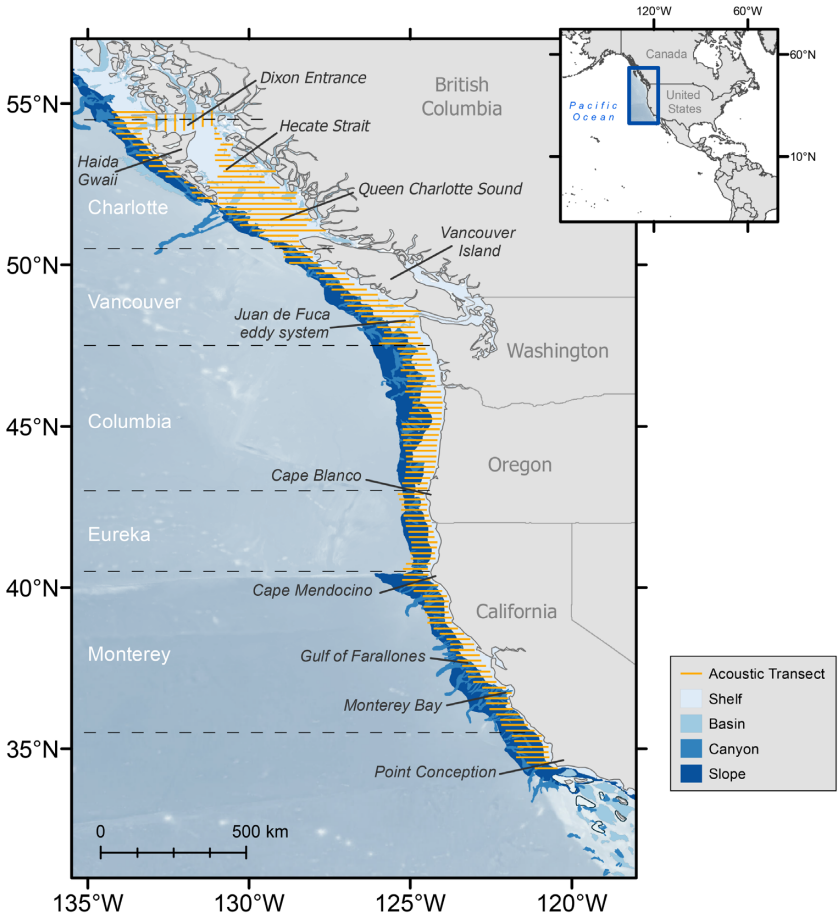

Figure 1. Study area along the west coast of the United States and Canada displaying bathymetric features and acoustic transect locations for a typical survey. Continental shelf habitat classifications are based on relief, from Harris *et al.* (2014). International North Pacific Fishery Commission (INPFC) geographical areas are labelled and separated by latitude with dashed lines. All geographic features mentioned in the text are also labelled.

Table 1. Summary of biennial joint US–Canada Integrated Ecosystem and Acoustic Trawl Surveys for Pacific hake used in this study by year, vessel, echosounder frequencies used, survey extent and date range, and total transects sampled by NOAA Fisheries Northwest Fisheries Science Center and DFO.

Year	Vessel	Echosounder frequencies	Min–max latitude	Start date	End date	Number of transects used in analyses
2007	MF (NOAA)	18, 38, 120, 200 (NOAA)	35.8–54.9	20-June	22-August	132 (NOAA)
2009	MF (NOAA), WER (DFO)	18, 38, 120, 200 (NOAA); 38, 120 (DFO)	35.7–54.7	30-June	6-September	77 (NOAA), 44 (DFO)
2011	SH (NOAA), WER (DFO)	18, 38, 70, 120, 200 (NOAA); 38, 120 (DFO)	35.2–54.9	26-June	10-September	83 (NOAA), 41 (DFO)
2012	SH (NOAA), WER (DFO)	18, 38, 70, 120, 200 (NOAA); 38, 120 (DFO)	35.8–55.3	27-June	7-September	73 (NOAA), 45 (DFO)
2013	SH (NOAA), WER (DFO)	18, 38, 70, 120, 200 (NOAA); 18, 38, 120 (DFO)	34.9–54.8	13-June	12-September	98 (NOAA), 36 (DFO)
2015	SH (NOAA), WER (DFO)	18, 38, 70, 120, 200 (NOAA); 18, 38, 120 (DFO)	32.7–55.1	20-June	8-September	89 (NOAA), 29 (DFO)
2017	SH (NOAA), NP (DFO)	18, 38, 120 (NOAA); 38, 120 (DFO)	34.5–54.8	25-June	8-September	94 (NOAA), 35 (DFO)
2019	SH (NOAA), NP (DFO)	18, 38, 70, 120, 200 (NOAA); 38, 120 (DFO)	34.4–54.8	17-June	13-September	78 (NOAA), 35 (DFO)

MF: Miller Freeman, WER: W.E. Ricker, SH: Bell M. Shimada, and NP: Nordic Pearl.

Krill identification and abundance estimation

To classify krill from acoustic backscatter, we used an algorithm developed by Gauthier *et al.* (Supplemental Material) that applies frequency differencing methods to differentiate krill from other acoustic targets based on their distinct frequency response using MVBS measured at 38 and 120 kHz (De Robertis *et al.*, 2010). The automated algorithm was developed using multi-frequency acoustic backscatter and associated net samples of *E. pacifica* and *T. spinifera* collected during several research surveys in waters off the west coast of Vancouver Island, British Columbia, Canada (Supplemental Material). Krill were identified by matching 120 kHz cells to 38 kHz cells in space and time using ping times and sample geometry, and then using a $\Delta MVBS_{120–38}$ range of 10.0–16.3 dB, which encompasses published frequency difference ranges calculated for krill in other parts of the North Pacific (McKelvey and Wilson, 2006; De Robertis *et al.*, 2010; Simonsen *et al.*, 2016). Matching cells with MVBS values less than a −70 dB

integration threshold at 120 kHz were excluded. All acoustic backscatter was treated as non-differentiated *E. pacifica* and *T. spinifera* because the frequency response of these two species overlaps at 38 and 120 kHz (Supplemental Material).

Georeferenced 120 kHz volumetric (S_v) and integrated area backscatter (nautical-area-backscattering coefficient, s_A or NASC, m^2 nmi^{-2}) attributed to krill were exported in 926 m (0.5 nmi) horizontal by 10 m vertical bins. To verify that the algorithm was correctly identifying krill and excluding targets such as swim-bladdered fish, maximum S_v values within each exported cell were examined at the transect level, and cells with S_v values in the 90th percentile of all values on the transect were scrutinized and corrected as needed to remove misclassifications (e.g. bottom intrusion). An additional 10% of transects in each year were randomly selected and visually scrutinized, with a focus on cells with high mean S_v values that were classified as krill. Reviewed files with corrections were then re-exported. We further limited our analyses to cells with MVBS values greater than −80 dB, which represents approximately 3–4 krill m^{-3} in each 926 m horizontal by 10 m vertical bin, assuming a target strength of −74.7 dB at 120 kHz (Miyashita *et al.*, 1996). We classed exported cells where MVBS values were less than −80 dB as empty water. This resulted in the removal of data from an additional 3.1% of cells across all years of the study. All subsequent analyses used integrated NASC values, which is an index of relative krill abundance and is a proxy for krill biomass.

Spatial variability

To ensure interannual comparisons of krill abundance and distribution were not biased by variation in survey extent, we limited our analyses to data that fell within the common latitudinal range of all years (35.8–54.7°N). To quantify interannual variation of krill distributions in the water column, we calculated mean NASC in each 10-m vertical bin along each transect for each year. We then calculated the weighted mean depth of krill and tested for differences among years using a one-way ANOVA (Zar, 1999). To obtain a measure of krill abundance through the water column, we summed NASC in each 10-m vertical bin for each 0.5-nmi horizontal cell, and aggregated data into 20 km (10.8 nmi) along-transect bins to minimize autocorrelation. We then examined interannual variation in mean NASC with a Kruskal–Wallis test (Zar, 1999). To examine variability in annual north–south krill distributions, we calculated the mean NASC in five regions defined for fisheries management by the International North Pacific Fishery Council (INPFC) based on latitude and oceanographic characteristics (Forrester *et al.*, 1983): Monterey (35.5–40.5°N), Eureka (40.5–43.0°N), Columbia (43.0–47.5°N), Vancouver (47.5–50.5°N), and Charlotte (50.5–54.5°N; Figure 1). We calculated the annual percentage of krill in each INPFC region, as well as the geographic center of gravity (COG) of krill as a measure of spatial variation in the 8-year time series.

To identify areas of greater of krill abundance, we used kernel density estimation (KDE) to create an annual density surface of krill using NASC in 20 km (10.8 nmi) along-transect bins. KDE is a simple non-parametric statistical technique that estimates a real-valued function as the weighted average of neighboring observed data (Worton, 1989). The weight is defined by the kernel, such that closer points are given greater weights, and smoothness is set by the kernel bandwidth. For this study we used a bandwidth of 50 km and 2000 cells to create the grid. We also used KDE to generate a map of krill density across the full time series, from 2007 to 2019.

Relationship to environmental conditions

To characterize krill abundance in relation to geomorphic features and environmental conditions, we compiled data on bathymetry, chl *a* concentration, and temperature. We used a seafloor geomorphic features map to examine krill relationships to bathymetric features including continental shelf (shallow seafloor < 200 m water depth), slope (narrow band of deepening seafloor from the continental shelf edge, ∼200–500 m water depth), shallow basins (seafloor depressions with closed bathymetric contours occurring on the continental shelf), and submarine canyons (steep-walled valleys that incise the slope; full definitions available from Harris *et al.*, 2014). In total, 45.2% (10 608 040 km^2) of the survey area was continental shelf habitat, 54.5% (12 790 233 km^2) was slope habitat, 0.19% (44 926 km^2) was submarine canyon habitat, and 0.07% (15 926 km^2) was shallow basin habitat (Harris *et al.*, 2014). Polygons of each bathymetric feature were spatially matched to the centroid of each 0.5 nmi cell, and krill in each 0.5 nmi cell were categorized as being associated with shelf, slope, basin, or canyon habitat. In a few cases, transects extended into offshore waters beyond the polygons used in this study; 0.5 nmi cells in this area were categorized as offshore-associated. We tested for differences in mean NASC in each habitat using a Kruskal–Wallis test, and *post hoc* Dunn test to determine which habitats were significantly different (Zar, 1999).

We obtained bottom depth values for the centroid of each 0.5 nmi cell using a composite bathymetry grid of the study domain in ArcMap (v.10.6; ESRI, Redlands, CA). The grids were created by combining three, 3-arc-second resolution Coastal Relief Models (Vols. 6–8; National Geophysical Data Center, 2003, 2013; Carignan *et al.*, 2013) with 15-arc-second resolution SRTM15 + data (Smith and Sandwell, 1997; Becker *et al.*, 2009; Sandwell *et al.*, 2014). National Geophysical Data Center (NGDC) Coastal Relief Models completely cover all land areas and consistently cover aquatic depths to approximately 2000 m. Deeper than 2000 m, NGDC data become inconsistent, so we filled in missing areas using resampled (to 3-arc-second) SRTM15 + data to obtain bottom depth values for the small number of transects that extended offshore into deeper waters. Using the same geomorphic features map from Harris *et al.* (2014), we measured the distance of the centroid of each 0.5-nmi cell to the edge of the nearest submarine canyon, shallow basin, and continental shelf break (200 m isobath).

To assess relationships between krill abundance and primary production, we accessed monthly composite chl *a* data (mg m^{-3}) from the Aqua MODIS satellite (NASA/GSFC OBPG, 2020) using the R packages "rerddap" and "rerddapXtracto" (Chamberlain, 2019; Simons, 2019; Mendelssohn, 2020). The centroid of each 0.5-nmi cell was assigned a single log-transformed chl *a* value based on the shortest distance between the center of the cell and the grid. We matched monthly composites of chl *a* grid values at 4 km resolution to the month of survey sampling to account for variation in primary production as the survey moved through the CCE from south to north, a range of approximately 2600 km.

To characterize temperatures experienced by krill within the water column, we used *in situ* temperature measured at a grid of sampling stations during each survey by temperature–depth profilers attached to trawl headropes, expendable bathythermographs, and conductivity–temperature–depth (CTD) instruments, as well as underway CTD measurements collected at sampling locations along transects (see Malick *et al.*, 2020 for full details). We used ordinary kriging (Cressie, 1993) to interpolate temperatures measured at a depth of 100 m to a 20 km^2 grid that encompassed all sampling locations across survey years, which allowed us to estimate annual temperature surfaces at depth. To remove the effect of latitude on temperature, we calculated grid-cell specific temperature anomalies by subtracting the average temperature for each grid cell across the 8-year time series from the annual temperature within each grid cell (Malick *et al.*, 2020). The centroid of each 0.5-nmi cell was assigned a single 100-m temperature anomaly value based on the shortest distance to the gridded surface of temperature anomalies.

To facilitate analyses on the same spatial scale, we gridded krill abundance data into 20 km^2 cells for further analyses and calculated mean values for distance to bathymetric features, bottom depth, chl *a*, and temperature. To examine variation in the two dynamic variables, chl *a* and temperature, we plotted the distribution of all values for each year and calculated the median value. For temperature, we used the median temperature anomaly in each year to classify ocean conditions as cool, neutral, or warm following Malick *et al.* (2020).

Statistical models

We developed hierarchical generalized additive models (or HGAMs; Pedersen *et al.*, 2019) using the mgcv package (Wood, 2006) in R (R Core Team, 2016) to examine relationships between krill abundance (20 km^2 cells) and environmental conditions. GAM models assume predictors have an additive effect and use smooth functions to model the effect of the predictors on the response variable (Wood and Augustin, 2002). HGAMs allow modelling of non-linear functional relationships between covariates and can account for within-group variability (Pedersen *et al.*, 2019). We modelled each response variable, krill presence and krill abundance (positive krill values) separately, and evaluated the influence of distance to the shelf break (km), distance to the nearest submarine canyon (km), bottom depth (m), chl *a* (mg m^{-3}, log scale; l_chla), and 100-m temperature anomaly (°C; temp_anom) on NASC. To account for interannual variability in spatial distributions, we included a spatial term (interaction of latitude and longitude), grouped by year. Both models were of the same general form. For the occurrence component we used a logistic model, where Z_i indicates the presence (1, NASC > 0) or absence (0, if NASC = 0) for the ith observation, and μ_i is the probability of occurrence [Equation (1)].

$$\begin{aligned} Z_i &\sim Bernoulli\left(\mu_i\right) \\ logit\left(\mu_i\right) &= year_i + te\left(lat_i, lon_i,\ by = year\right) + s\left(shelf_i\right) \\ &\quad + s\left(canyon_i\right) + s\left(depth_i\right) + s\left(l\_chla_i\right) \\ &\quad + s\left(temp\_anom_i\right). \end{aligned} \tag{1}$$

For the positive component of the model, we modelled the observed krill abundance, Y_i, using a gamma likelihood with a log-link, modelling the mean abundance, φ_i, conditional on krill presence [Equation (2)].

$$\begin{aligned} Y_i &\sim Gamma\left(\varphi_i, \gamma\right) \\ log\left(\varphi_i\right) &= year_i + te\left(lat_i, lon_i,\ by = year\right) + s\left(shelf_i\right) \\ &\quad + s\left(canyon_i\right) + s\left(depth_i\right) + s\left(l\_chla_i\right) \\ &\quad + s\left(temp\_anom_i\right). \end{aligned} \tag{2}$$

In both models, $year_i$ is a factor for survey year, $s()$ indicates the smooth effect of each covariate, and $te()$ indicates a tensor-product smooth for the two covariates. Thin plate regression splines were used as smoothing functions, and spline shrinkage was used to perform automatic smoothness selection of covariates. We restricted the number of basis functions contributing to each smooth by limiting the number of polynomial curve joins, or knots ($k = 5$ for all smooths, see *mgcv* package, Wood, 2006). Inspection of smooth terms revealed partial effects that were biologically reasonable and avoided overfitting (i.e. excessive wiggliness). We evaluated a range of models, including models without the spatial term, and used deviance explained, changes in Akaike's information criterion (ΔAIC), and Akaike weights (ωi) to select best-fit models (Akaike, 1998). Normalized residuals were plotted to check for violations of model assumptions. The partial effect of each covariate retained in each final model was plotted to examine the relationship. The final models were then used to predict probability of krill occurrence (μ) and abundance conditioned on presence (φ). We generated an unconditional prediction for krill abundance, X, by multiplying the occurrence and positive components (i.e. $X = \mu * \varphi$). All analyses were performed using R software version 3.6.2 (R Core Team, 2016).

Results

Krill aggregations were distributed between 50 and 300 m in the water column (Figure 2), with an average depth of 148 ± 44 m that did not vary significantly among years ($F_{7,192} = 0.734$, $p = 0.643$). While krill depth distributions were stable, abundance varied spatially along the coast and among years ($H_7 = 177.3, p < 0.001$; Figure 3a). Mean NASC was lowest in 2015 (59.3 ± 371.0 m^2 nmi^{-2}), and greatest in 2013 (198.7 ± 698.0 m^2 nmi^{-2}; Figure 3b). On average, krill were relatively evenly distributed within INPFC geographic areas, with a mean of 58.6% of krill occurring in US areas, and 41.4% occurring in Canadian areas (Figure 3b). While krill abundance was very low in 2015 throughout most of US west coast waters, krill abundance was high in Canadian west coast waters, where 90.6% of krill were located, including 76.5% in the northernmost INPFC area in our study (Charlotte; Figure 3b). As a result, the geographic COG was located farther north in 2015 compared to other years (Figure 3a). In contrast, in 2009 only 21.6% of krill were located in Canadian west coast waters, and greatest abundances were located in the southernmost INPFC area in our study (Monterey; Figure 3b), resulting in a southerly shift in the geographic COG (Figure 3a).

The location of greatest kernel density estimates (KDE) of krill was also variable (Figure 4). When all years were aggregated, increased density estimates were located in the area between Cape Mendocino in northern California and Cape Blanco in southern Oregon, and the Juan de Fuca eddy system near the border between the United States and Canada

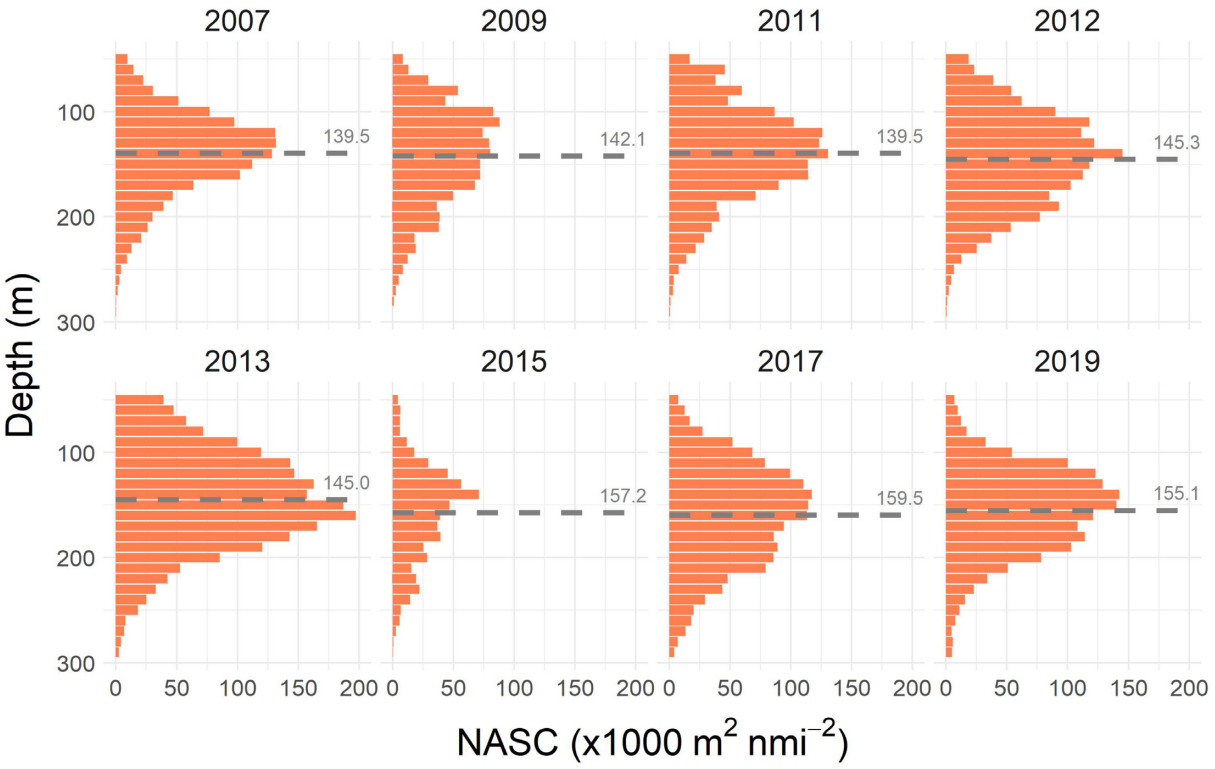

Figure 2. Annual depth distribution of krill abundance (NASC) in the 8-year time series. Data are presented in 10-m vertical depth bins. Labelled dashed lines indicate the weighted mean depth of krill within each year.

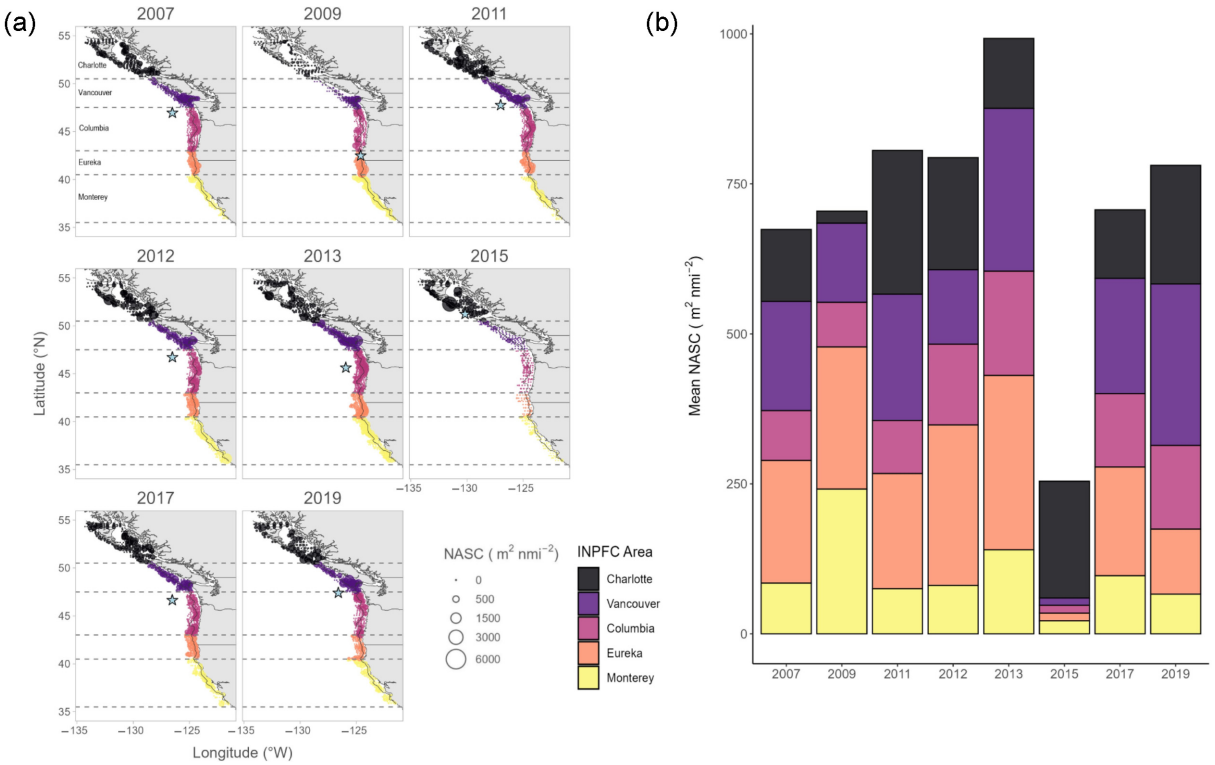

Figure 3. Spatial distribution of krill abundance (NASC) observed during joint US–Canada Integrated Ecosystem and Acoustic Trawl Surveys for Pacific hake during 2007–2019, including (a) NASC in binned 20-km cells along transects, with blue stars representing the geographic COG and dashed lines and separate colours delineating each International North Pacific Fishery Commission (INPFC) geographical area; and (b) mean annual NASC in each INPFC area.

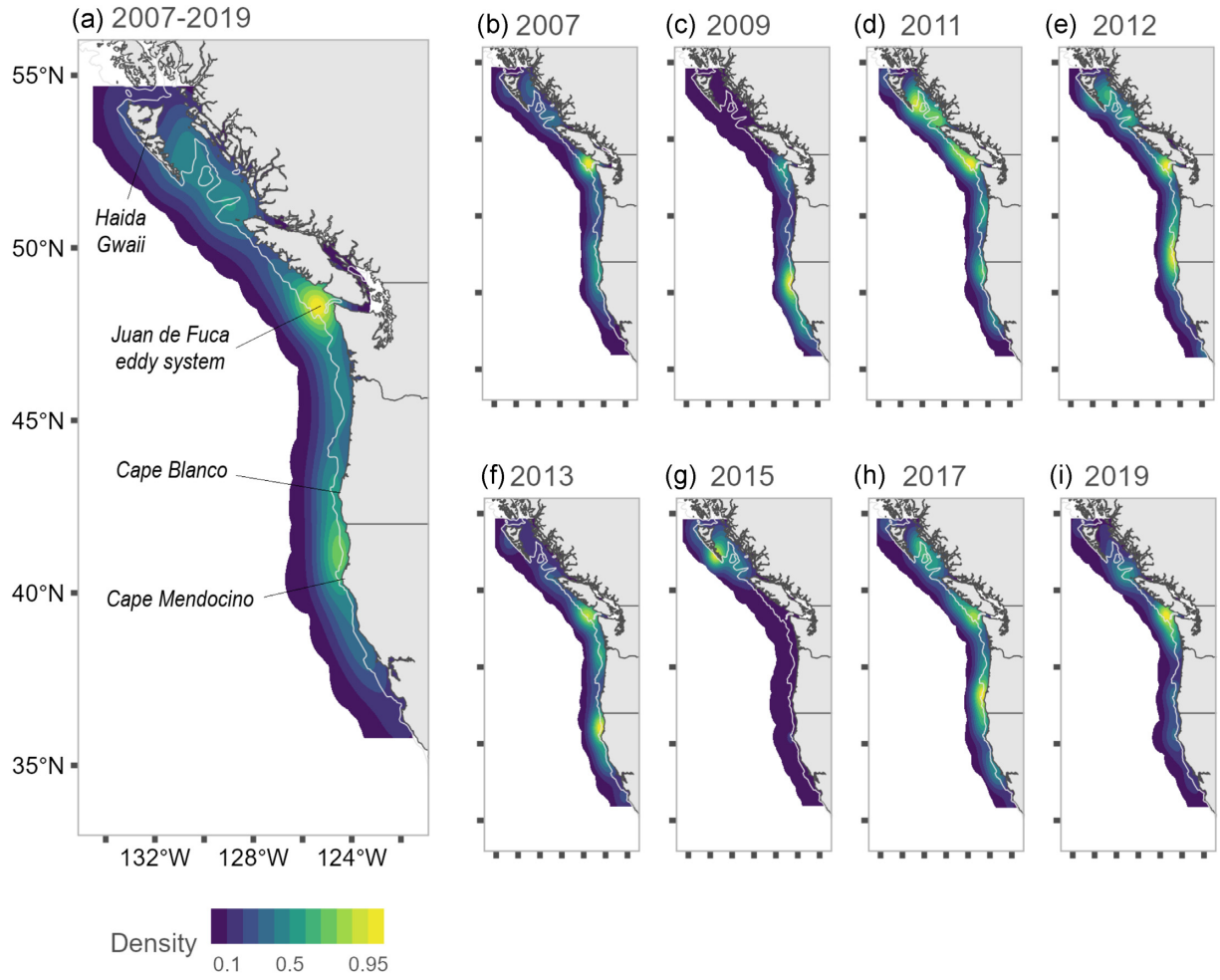

Figure 4. KDE of krill distribution based on NASC (a) across all years in the time series, and (b)–(i) each individual year. KDE results are shown on a standardized (0–1) scale.

(Figure 4a). However, when analyzing each year separately, KDE indicated that increased krill abundances were located in different areas along the coast. For example, increased krill density estimates occurred near the shelf break off the Oregon coast in 2011, 2012, 2013, and 2017 (Figure 4d–f and h), and in waters near Haida Gwaii in 2011 and 2015 (Figure 4d and g).

Krill were observed in a range of bathymetric habitats, with greatest NASC values in shallow basins and on the continental shelf, followed by submarine canyons and slope habitat (Figure 5). Mean NASC was significantly different among all habitats ($H_4 = 460.49$, $p < 0.001$), except between slope and canyon habitats (Dunn's test, $p = 0.587$).

Coast-wide median temperature anomalies were lower than −0.1°C in 4 of the 8 years of our study (2007, 2009, 2012, and 2013), and were classified as cool (Figure 6a). The median temperature anomaly in 2011 was −0.07°C, and classified as neutral. The three most recent years in the time series (2015, 2017, and 2019) all had median temperature anomalies greater than +0.3°C, which we classified as warm ocean conditions. In comparison to variation in temperature anomalies, chl *a* concentrations were less variable and the median value of chl *a* was above 0.46 mg m^{-3} (log scale) in all years (Figure 6b).

Krill were present in 53.2% of the gridded 20 km^2 cells used in our analyses. HGAM models of krill presence and positive values indicated a significant effect of annual spatial variability (spatial interaction term retained in final models, Table 2). Plots of partial effects indicated similar relationships between krill presence and positive values (Figures 7 and 8), and all covariates had a significant effect (Table 2). Proximity to the continental shelf break (within 20 km) and shallower bottom depths (< 750 m) had the strongest influence on krill, while proximity to submarine canyons exhibited a weak influence. Intermediate values of chl *a* concentration (~1 mg m^{-3}, log scale) had a significant effect on krill presence, and a slight influence on krill positive values. Temperature anomalies at a depth of 100 m had a significant influence on krill presence, with temperature anomalies above 0°C having a negative effect on krill in both models.

Based on the HGAM results, predictions of unconditional krill abundance showed generally similar patterns between years for bathymetric covariates, with abundance predicted to be highest within 10–20 km of the shelf break (Figure 9). In 2015, krill abundances were predicted to be greatest slightly off the shelf compared to other years. Predictions of krill abundance in relation to submarine canyons were greatest ~10 km from submarine canyons. Greatest abundances of krill were consistently predicted to occur in areas with bottom depths

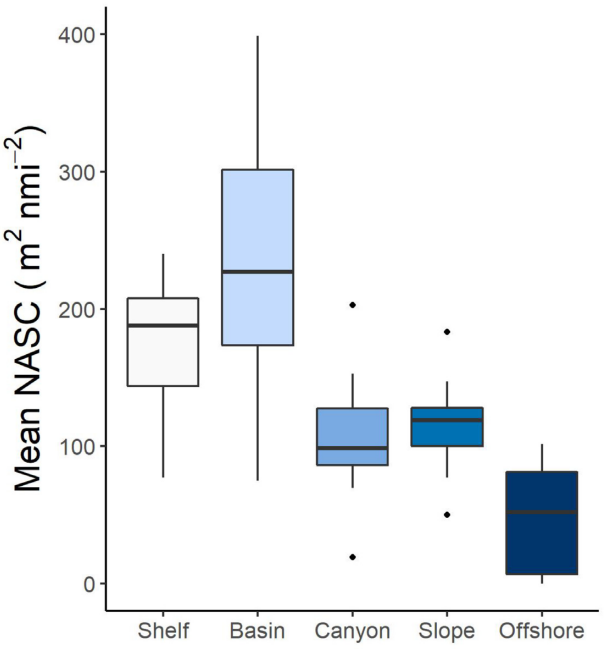

Figure 5. Distribution of annual mean krill abundances (NASC) in each bathymetric habitat. Boxplot—dark line: median; box: interquartile range (IQR); error bars: max/min within 1.5 × IQR above/below IQR; and dots: outliers.

of ∼300 m, with the exception of 2009 and 2012 when krill abundance was greatest in waters of depths of ∼700 m (Figure 9). In terms of dynamic covariates, greatest krill abundances were predicted at intermediate values of chl *a* (between 0.5 and 2.0 mg m^{-3}, log scale). Interestingly, peaks in krill abundance in 2013 and 2015, years with the highest and lowest abundances in our study, were associated with lower chl *a* values (∼0.25 mg m^{-3}, log scale). In contrast, predictions of krill varied substantially in relation to temperature anomalies. We found that unconditional krill abundance was predicted to be greatest during periods when temperature anomalies were below 0°C, or cool ocean conditions, with a peak in predicted abundance when temperature anomalies were approximately −0.2°C. When temperature anomalies were greater than 0°C, during warm ocean conditions, unconditional krill abundances generally declined.

Discussion

Using an archived fisheries acoustics dataset, we developed a time-series of coast-wide krill abundance and distribution in the CCE. We demonstrated that while krill vertical distributions were stable across the eight surveys, with an average depth of 148 m, overall abundances and spatial distributions varied substantially along the US and Canadian west coasts. Krill aggregations were primarily located near the Juan de Fuca eddy system and the region between Cape Mendocino, California, and Cape Blanco, Oregon, and to a lesser extent near the shelf break in Oregon, and Haida Gwaii and Queen Charlotte Sound, British Columbia. Variation in temperature exhibited the strongest influence on krill abundance, and lowest abundances were observed in 2015 during a marine heat wave. Bathymetry was also an important factor, and greatest krill abundance occurred in waters shallower than 400 m near the shelf break and associated with shallow basin habitats. This study provides insights into the spatiotemporal variation of krill in the CCE and relationships to environmental conditions, which will be useful for future studies of krill populations in a changing environment.

Our results demonstrate that krill presence and abundance was strongly associated with continental shelf habitats, particularly within 20 km of the shelf break. This pattern occurred regardless of continental shelf width, which can be very narrow in the southern part of the California Current, and wider along the Washington and British Columbia coast. Areas with sharp changes in bathymetry, such as near the continental shelf break, as well as basin and submarine canyon edges, are known to support krill populations (Mackas, 1992; Peterson *et al.*, 2000; Santora *et al.*, 2018). Dynamic mixing of cold, nutrient-rich waters along these bathymetric gradients gener-

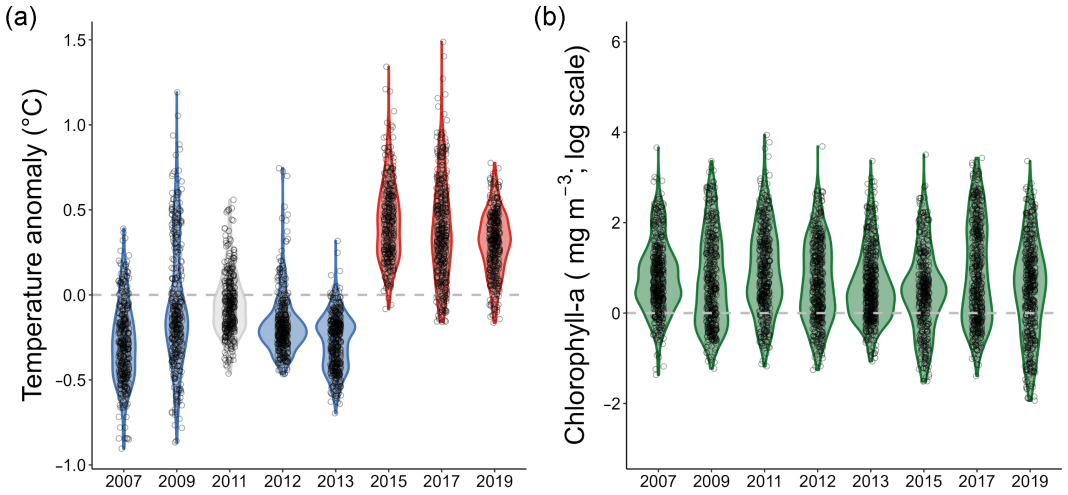

Figure 6. Annual distribution of (a) anomalies from the mean temperature (°C) at a depth of 100 m, and (b) chl *a* concentration (mg m^{-3}; log scale). For the temperature plots, blue shading indicates that the median temperature anomaly was below −0.1°C, which we classified as cool ocean conditions; red shading indicates that the median anomaly was above +0.3°C, which we considered warm ocean conditions; and grey shading in 2011 indicates that the median anomaly was between −0.1°C and 0.1°C, considered neutral ocean conditions (Malick *et al.*, 2020). For the chl *a* plots, median values were greater than 0.46 mg m^{-3} in all years, indicated by green shading.

Table 2. Description of HGAMs developed to evaluate the influence of bathymetric and environmental covariates on krill presence and krill non-zero abundance (NASC). For each model formulation tested, the corresponding effective degrees of freedom (edf), deviance explained, AIC and differences (ΔAIC), and ωi are presented. Final models are in bold.

Model description	Model name	Model construction	edf	Deviance explained	AIC	ΔAIC	ω_i
Krill presence with spatial interaction	**kp.1**	**Full model**	**88.8**	**25.1**	**2679.3**	**0.0**	**0.99**
	kp.2	Drop chl *a*	85.9	24.1	2712.3	33.0	6.9E-08
	kp.3	Drop bottom depth	86.8	20.9	2824.5	145.2	2.9E-32
	kp.4	Drop temp anomaly	78.6	17.9	3562.2	882.9	1.9E-192
	kp.5	Drop distance to canyon	83.0	18.2	3558.9	879.6	1.0E-191
	kp.6	Drop shelf distance	71.5	9.6	3890.4	1211.1	1.0E-263
	kp.7	Drop spatial interaction term	8.0	2.9	4038.8	1359.5	6.0E-296
Krill presence with only latitude	kp.1l	Full model	51.6	20.3	2764.5	85.2	3.2E-19
	kp.2l	Drop chl *a*	56.5	20.5	2774.7	95.4	1.9E-21
	kp.3l	Drop bottom depth	46.1	16.1	2903.6	224.3	2.0E-49
	kp.4l	Drop temp anomaly	48.9	15.3	3610.1	930.8	7.5E-203
	kp.5l	Drop distance to canyon	50.8	15.3	3612.7	933.4	2.0E-203
	kp.6l	Drop shelf distance	43.1	7.4	3924.4	1245.1	4.3E-271
Krill presence with no spatial interaction	kp.1s	Full model	27.4	16.4	2846.9	167.6	4.1E-37
	kp.2s	Drop chl *a*	23.8	15.8	2868.2	188.9	9.3E-42
	kp.3s	Drop bottom depth	19.8	12.0	2988.4	309.1	7.5E-68
	kp.4s	Drop temp anomaly	15.8	10.9	3726.3	1047.0	4.4E-228
	kp.5s	Drop distance to canyon	12.0	10.4	3739.5	1060.2	5.9E-231
	kp.6s	Drop shelf distance	31.6	6.6	3936.5	1257.2	1.0E-273
Krill abundance with spatial interaction	**kd.1**	**Full model**	**113.6**	**29.8**	**27509.3**	**0.0**	**1.00**
	kd.2	Drop chl *a*	111.3	29.7	27551.6	42.3	6.5E-10
	kd.3	Drop bottom depth	103.7	27.9	27612.8	103.5	3.3E-23
	kd.4	Drop temp anomaly	104.5	25.7	33934.7	6425.4	0.0
	kd.5	Drop distance to canyon	88.5	24.4	33968.8	6459.5	0.0
	kd.6	Drop shelf distance	81.9	17.7	34280.2	6770.9	0.0
	kd.7	Drop spatial effect	9.0	1.8	34814.9	7305.6	0.0
Krill abundance with only latitude	kd.1l	Full model	78.1	29.8	27620.6	111.3	6.6E-25
	kd.2l	Drop chl *a*	75.1	29.7	27669.7	160.4	1.5E-35
	kd.3l	Drop bottom depth	69.7	27.9	27700.1	190.8	3.6E-42
	kd.4l	Drop temp anomaly	67.4	25.7	34104.7	6595.4	0.0E + 00
	kd.5l	Drop distance to canyon	56.4	24.4	34117.8	6608.5	0.0E + 00
	kd.6l	Drop shelf distance	46.4	17.7	34444.5	6935.2	0.0E + 00
Krill abundance with no spatial interaction	kd.1s	Full model	25.7	29.8	27975.9	466.6	4.8E-102
	kd.2s	Drop chl *a*	22.2	29.7	28020.9	511.6	8.0E-112
	kd.3s	Drop bottom depth	18.4	27.9	28027.8	518.5	2.6E-113
	kd.4s	Drop temp anomaly	15.4	25.7	34479.5	6970.2	0.0E + 00
	kd.5s	Drop distance to canyon	12.7	24.4	34479.0	6969.7	0.0E + 00
	kd.6s	Drop shelf distance	9.0	17.7	34814.9	7305.6	0.0E + 00

ates phytoplankton blooms that krill consume. Wind relaxation events, which often follow periods of strong upwelling, can maintain primary production in areas that are accessible by krill for longer periods of time (Ressler *et al.*, 2005). The relationship between NASC and bottom depth also indicated strong associations with waters near the shelf break and slightly deeper slope waters (200–400 m). Water depths just beyond the shelf break can increase rapidly to greater than 750 m, and krill occupying the shelf break habitat can easily be advected away from areas with strong currents (Dorman *et al.*, 2011), which may explain the distribution of krill in a wide range of bottom depths.

Increased krill abundance also occurred near shallow basins and to a lesser extent near shelf-incising submarine canyons, which can be found along the west coast of the United States and Canada (Mackas *et al.*, 1997; Santora *et al.*, 2018). While the overall area of shallow basins surveyed in this study was less than 1% of the survey area, these habitats supported the greatest mean NASC values. In comparison, krill abundances in submarine canyons were not as high, and there was not a strong relationship between NASC and proximity to submarine canyons. Nearly all of the submarine canyons in this study were located in US waters, and comprised less than 0.2% of the survey area. The weak relationship to submarine canyons observed in our study, as compared to other recent research (Santora *et al.*, 2018), may be a result of the fisheries survey design, our focus on broad, coast-wide descriptions of krill distributions, and the approach to aggregate data onto a 20 km^2 grid. The lack of krill aggregations in central California near Monterey Bay and the Gulf of the Farallones also contrasts with previous research (Santora *et al.*, 2011; Fiechter *et al.*, 2020) and may relate to the timing of our survey and the inherent spatiotemporal variability of krill distributions (Evans *et al.*, 2021). The phenology of krill hotspot formation and dissolution can vary substantially depending on local changes in upwelling activity (Ressler *et al.*, 2005; Fiechter *et al.*, 2020; Evans *et al.*, 2021), and our results may not represent intraseasonal variation in krill distributions. A closer examination of krill abundance at a finer spatial resolution within regions where a large number of canyons occur, and near lo-

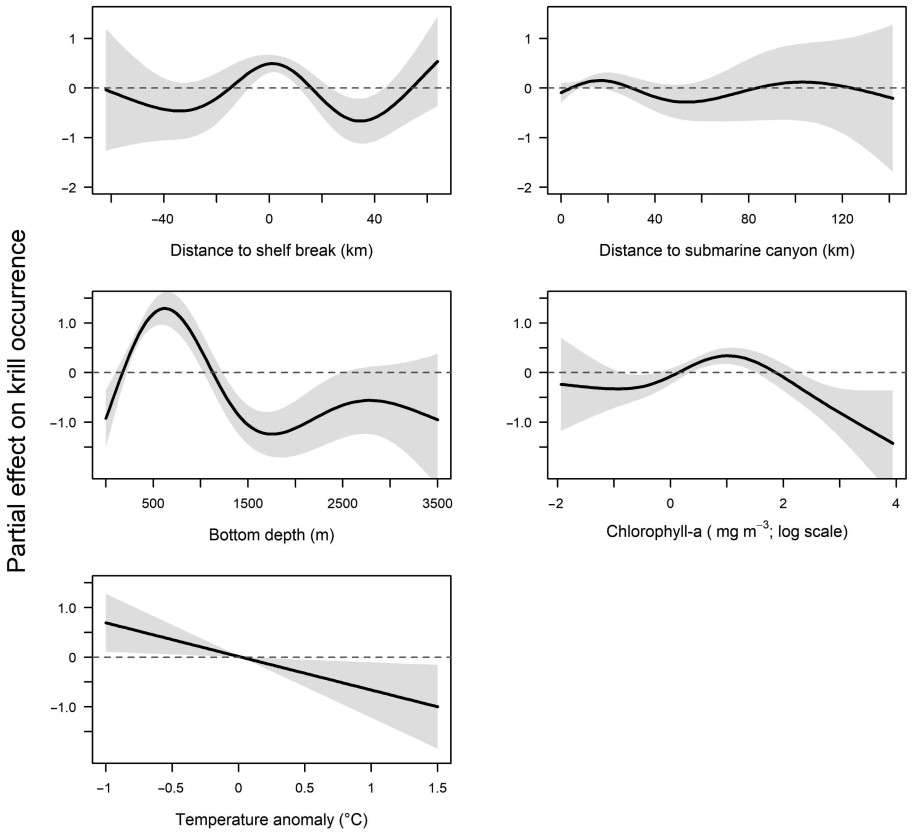

Figure 7. Partial effects plots of smooth functions in the HGAM model of krill presence. Grey shading around smooth fits represents 95% *CI*s.

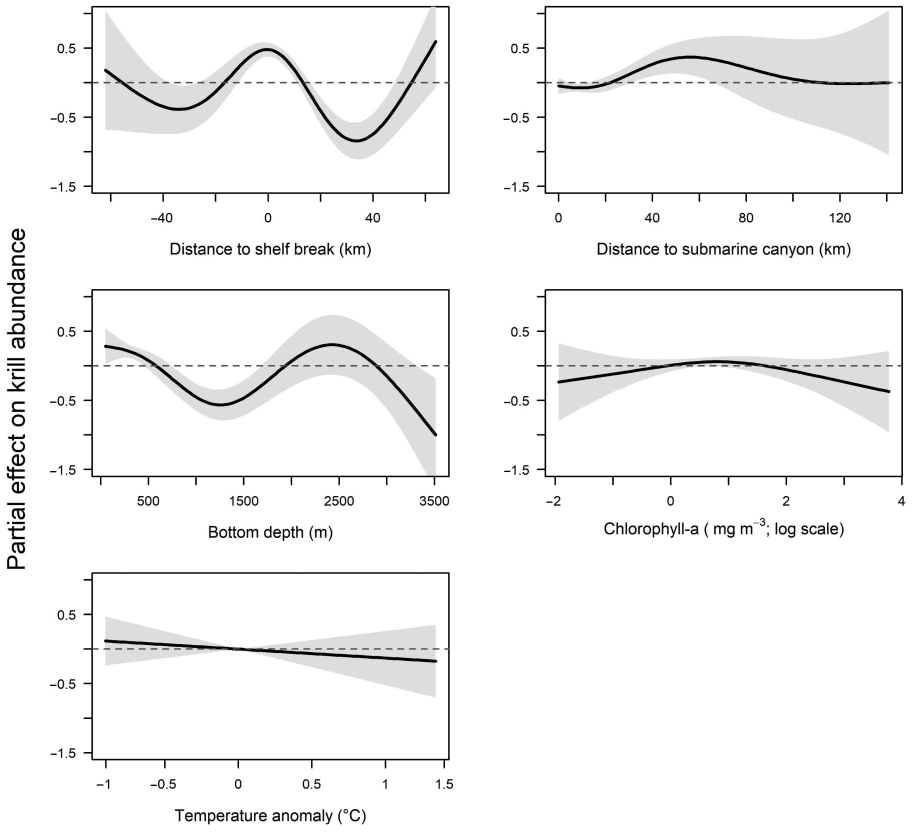

Figure 8. Partial effects plots of smooth functions in the HGAM model of krill abundance (NASC) conditioned on presence. The model used a log-link for NASC. Grey shading around smooth fits represents 95% *CI*s.

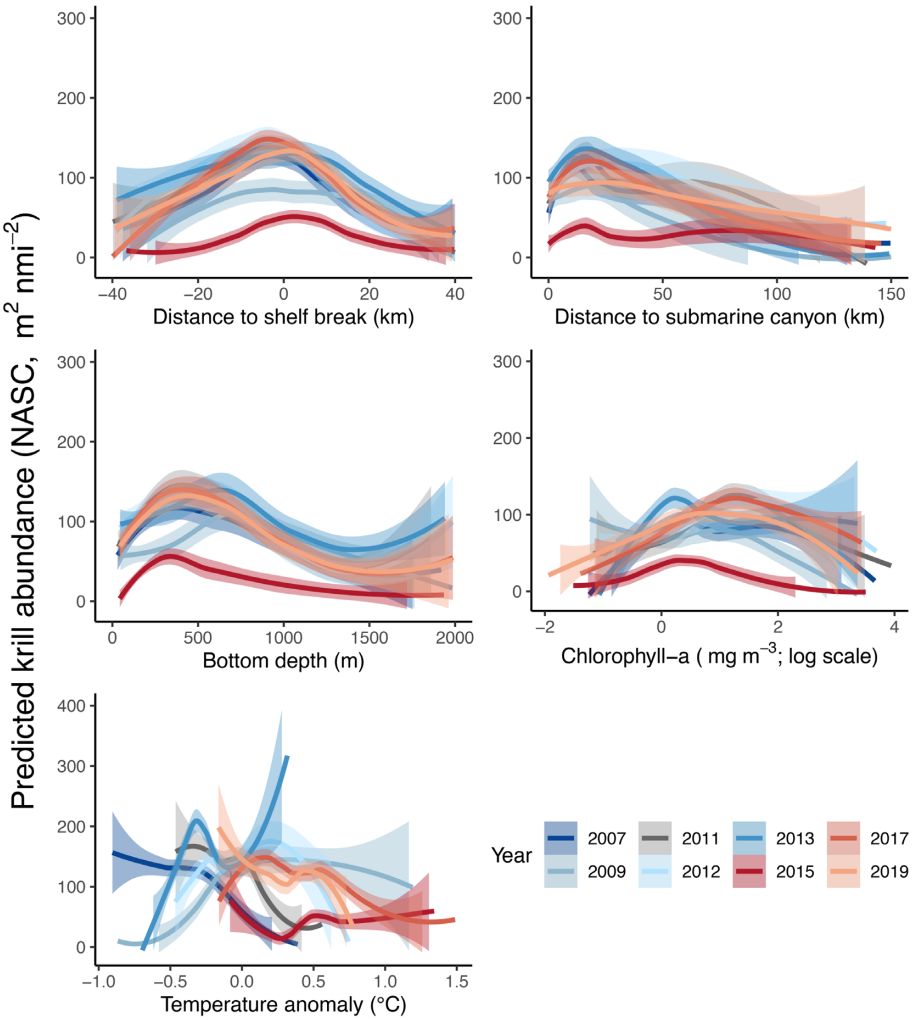

Figure 9. Unconditional krill abundance predictions for each of the covariates included in the final HGAM models. Each year is coloured based on the annual median temperature anomaly (°C) at depths of 100 m across the study area. Blue shading indicates that the median temperature was below −0.1°C, red shading indicates that the median temperature was above + 0.3°C, and grey shading indicates that the median anomaly was between −0.1 and 0.1°C.

cations where previous studies have identified krill hotspots, may reveal stronger habitat relationships. Regardless, our results highlight the importance of shallow ocean basin habitats for krill, and suggest that in areas where there are fewer submarine canyons, such as the west coast of British Columbia and the southernmost portion of the CCE near the Southern California Bight (which was not part of this study), shallow basins can also support dense krill aggregations (Fiedler *et al.*, 1998).

Temperature anomalies at 100-m showed marked variability, with cooler conditions occurring in the first part of our time series (2007, 2009, 2012, and 2013) and warmer conditions occurring during the three most recent years (2015, 2017, and 2019). This is in contrast to chl *a* concentrations, which were not as variable across years. Relationships between krill abundance and chl *a* were relatively consistent across the time series, whereas temperature effects were evident in declines in krill abundance and shifts in their spatial distribution. We confirmed that the extended marine heat wave, or "Blob" (Leising *et al.*, 2015; Di Lorenzo and Mantua, 2016), negatively impacted krill abundance along the US west coast in 2015, and can explain the observed ecological impacts within the rest of the CCE food web, including a widespread seabird die-off (Peterson *et al.*, 2017; Jones *et al.*, 2018). We did not detect a significant shift in the depth of krill in 2015, which were located in an average of 157 m water, indicating that krill did not move to deeper waters when surface waters were warm. Interestingly, krill abundance in the northernmost part of our survey area (British Columbia) were above average during 2015. Local ocean currents and greater primary productivity, perhaps related to a shift in the location of the bifurcation of the North Pacific Current (Sydeman *et al.*, 2011; Malick *et al.*, 2016), or the influence of a shallow shelf and multiple shallow basins, may have sustained krill populations in this part of the study area during the marine heat wave.

While we demonstrated that temperature anomalies had a significant impact on annual krill abundances, shifts in the location and timing of upwelling and subsequent primary production also appear to play an important role. For example, 2017 and 2019 were also anomalously warm years (Amaya *et al.*, 2020; Malick *et al.*, 2020, this study), yet krill abundances did not show significant declines, and were closer to pre-2015 abundances, with aggregations located in both US and Canadian waters. Thus, krill populations appear to be able to take

advantage of primary productivity even during warmer ocean temperatures, which may become more common in the future (Di Lorenzo and Mantua, 2016). Predictions of krill population dynamics should account for the interaction of multiple drivers including temperature and primary production on krill abundance and distribution (McHenry *et al.*, 2019). It should be noted that the warmer ocean conditions observed during 2017 and 2019 were not as extensive as the 2014–2016 marine heat wave, which was unprecedented in terms of spatial extent and duration (Di Lorenzo and Mantua, 2016; Jacox *et al.*, 2018). Future large-scale and long duration marine heat waves may have similarly negative consequences for krill populations along the US and Canadian west coasts. Additionally, we did not directly examine cross-shelf transport, upwelling, or mesoscale circulation, but the high degree of spatial resolution in our dataset provides future opportunities for regionally focused studies of krill abundance that incorporate regional oceanographic circulation models (Neveu *et al.*, 2016) or *in situ* measures of current strength and direction.

For mobile krill predators, the ability to migrate throughout CCE waters may provide an advantage that increases access to variable prey resources during the summer months. Because an average of 41% of krill observed in this study occurred in Canadian waters, northerly migrations may impart a particularly significant increase in survival, especially when krill abundances are low in the southern part of the CCE. During the 2015 marine heat wave, krill abundance was greatest in northern British Columbia (Charlotte INPFC region), whereas in other years, greatest densities occurred in California waters (Monterey INPFC region). The northern extent of hake migrations is related to poleward transport and warm ocean conditions (Agostini *et al.*, 2006), and our findings suggest that this may be related to increased densities of krill in the northern California Current, particularly Canadian coastal waters (Benson *et al.*, 2002). Similarly, blue whales migrating from the south appear to use memory to locate predictably productive areas in the CCE to forage (Abrahms *et al.*, 2019), which may include krill aggregations between Cape Mendocino and Cape Blanco identified in this study. Further research on relationships between predator distributions and krill abundance will provide a better understanding of interannual variation in the migratory extent of krill-dependent predators.

Ideally, acoustic surveys for zooplankton are paired with ground truth data to confirm species identifications and quantify biological information including size, developmental stage, and reproductive status. Because we used archived acoustic data that were collected for Pacific hake stock assessment purposes, direct samples of krill aggregations for species-level identification were not available. We are confident that our classification algorithm correctly discriminated *E. pacifica* and *T. spinifera* from other zooplankton (Supplemental Material). Nonetheless, the overlapping spatial distributions and frequency response of these two krill species may have confounded some of our results. Specifically, *E. pacifica* are widespread near the shelf-break and in offshore waters, while *T. spinifera* are neritic and typically occur in shallower, coastal shelf waters (Brinton, 1962; Peterson *et al.*, 2000). The relationship of distance to the continental shelf break indicated a greater probability of krill either inshore or offshore of the shelf break, which may reflect fine-scale differences in distributions of these two species that we could not discern in the acoustic data. Furthermore, there is evidence that *T. spinifera* are more common in British Columbia compared to *E. pacifica* (Brinton, 1962), and therefore, some of the spatiotemporal variation in our dataset may be due to species-specific differences in abundance in response to local ocean conditions, particularly in northern British Columbia (Evans *et al.*, 2021). While net sampling can introduce biases related to escapement and net avoidance that requires additional methodological considerations (Greene *et al.*, 1998; McClatchie *et al.*, 2000; Skjoldal *et al.*, 2013), future research that uses fisheries acoustics data coupled with *in situ* sampling to confirm krill species identification will allow for studies of species-level abundance and distribution patterns.

Long-term ecological time series are critical for a better understanding of ecosystem variation, the development of a mechanistic understanding of ecological relationships, and to inform ecosystem-based management (Harvey *et al.*, 2020). By utilizing existing acoustic data collected from a systematic fisheries assessment survey of the CCE, we generated biennial estimates of coast-wide krill abundance that represent a valuable source of information on ecosystem status. Furthermore, by quantifying krill–environment relationships we contribute to a broader understanding of the influence of ocean conditions on a key component of the CCE food web. This novel time series presents additional research opportunities, including the development of forecasts of how changing ocean conditions may affect krill populations and krill-dependent predators under a warming and increasingly variable ocean environment (Sydeman *et al.*, 2013). This 8-year time series will be updated as new acoustic data are collected and estimates of krill abundance become a standard output of the joint US–Canada Integrated Ecosystem and Acoustic Trawl Surveys for Pacific hake, thus providing an ongoing source of information about krill abundance in the CCE.

Funding

Funding was provided by NOAA's Fisheries and the Environment (FATE) program to support EMP through a National Academy of Science/ National Research Council postdoctoral award (grant number 18-02).

Supplementary data

Supplementary material is available at the ICESJMS online.

Authors' contributions

SPS, DC, SG, RT, AOS, and EMP conceived of this work, and acquired, processed, and interpreted the data. EMP drafted the manuscript, and EMP, SPS, DC, SG, RT, and AOS revised the manuscript. All authors approve of the submitted version.

Data availability statement

The raw acoustic data underlying this article are available from the National Centers for Environmental Information, https://www.ncei.noaa.gov/. Processed data will be made available through the NOAA Fisheries, Northwest Fisheries Science Center, and are currently available by request to the corresponding author.

Acknowledgements

We thank the captains and crew of the vessels used to conduct the acoustic trawl surveys. We thank J. Nephin and C. Stanley for assistance with acoustic processing scripts and classification templates for krill, and J. Pohl for assistance with temperature data processing. B. Feist provided data to create the bathymetric maps. J. Clemons, M. Haltuch, C. Harvey, M. Jacox, M. Malick, K. Marshall, and N.Tolimieri contributed valuable insights and comments during this project. We also thank C. Vestfals and three anonymous reviewers for useful comments on our manuscript. Author order is alphabetical after first author.

References

Abrahms, B., Hazen, E. L., Aikens, E. O., Savoca, M. S., Goldbogen, J. A., Bograd, S. J., Jacox, M. G. *et al.* 2019. Memory and resource tracking drive blue whale migrations. Proceedings of the National Academy of Sciences, 19: 5582–5587.

Agostini, V. N., Francis, R. C., Hollowed, A. B., Pierce, S. D., Wilson, C., and Hendrix, A. N. 2006. The relationship between Pacific hake (*Merluccius productus*) distribution and poleward subsurface flow in the California Current System. Canadian Journal of Fisheries and Aquatic Sciences, 63: 2648–2659.

Akaike, H. 1998. Information theory and an extension of the maximum likelihood principle. *In* Selected Papers of Hirotugu Akaike, pp. 199–213. Ed. by E. Parzen, K. Tanabe, and G. Kitagawa. Springer, New York, NY. https://doi.org/10.1007/978-1-4612-1694-0_15 (last accessed 26 August 2021).

Amaya, D. J., Miller, A. J., Xie, S.-P., and Kosaka, Y. 2020. Physical drivers of the summer 2019 North Pacific marine heatwave. Nature Communications, 11: 1–9.

Becker, J. J., Sandwell, D. T., Smith, W. H. F., Braud, J., Binder, B., Depner, J., Fabre, D. *et al.* 2009. Global bathymetry and elevation data at 30 arc seconds resolution: SRTM30_PLUS. Marine Geodesy, 32: 355–371.

Benson, A. J., McFarlane, G. A., Allen, S. E., and Dower, J. F. 2002. Changes in pacific hake (*Merluccius productus*) migration patterns and juvenile growth related to the 1989 regime shift. Canadian Journal of Fisheries and Aquatic Sciences, 59: 1969–1979.

Brinton, E. 1962. The distribution of Pacific euphausiids. Bulletin of the Scripps Institution of Oceanography, 8: 51–270.

Brinton, E., and Townsend, A. 2003. Decadal variability in abundances of the dominant euphausiid species in southern sectors of the California Current. Deep Sea Research Part II Topical Studies in Oceanography, 50: 2449–2472.

Carignan, K. S., Eakins, B. W., Love, M. R., Sutherland, M. G., and McLean, S. J. 2013. Bathymetric Digital Elevation Model of British Columbia, Canada: Procedures, Data Sources, and Analysis. NOAA National Geophysical Data Center (NGDC), Boulder, CO. https://wiki.oceannetworks.ca/download/attachments/48694705/British_Columbia.pdf?api=v2 (last accessed: January 17, 2020).

Chamberlain, S. 2019. rerddap: general purpose client for 'ERDDAP' servers. https://CRAN.R-project.org/package=rerddap (last accessed: April 29, 2020).

Checkley, D. M., and Barth, J. A. 2009. Patterns and processes in the California Current System. Progress in Oceanography, 83: 49–64.

Cimino, M. A., Santora, J. A., Schroeder, I., Sydeman, W., Jacox, M. G., Hazen, E. L., and Bograd, S. J. 2020. Essential krill species habitat resolved by seasonal upwelling and ocean circulation models within the large marine ecosystem of the California Current System. Ecography, 43: 1–15.

Cressie, N. 1993. Statistics for Spatial Data, revised edition. John Wiley & Sons, Inc., Hoboken, NJ. 928pp. doi: 10.1002/9781119115151.

Croll, D. A., Tershy, B. R., Hewitt, R. P., Demer, D. A., Fiedler, P. C., Smith, S. E., Armstrong, W. *et al.* 1998. An integrated approach to the foraging ecology of marine birds and mammals. Deep Sea Research Part II Topical Studies in Oceanography, 45: 1353–1371.

De Robertis, A., and Higginbottom, I. 2007. A post-processing technique to estimate the signal-to-noise ratio and remove echosounder background noise. ICES Journal of Marine Science: Journal du Conseil, 64: 1282–1291.

De Robertis, A., McKelvey, D. R., and Ressler, P. H. 2010. Development and application of an empirical multifrequency method for backscatter classification. Canadian Journal of Fisheries and Aquatic Sciences, 67: 1459–1474.

Demer, D. A., Berger, L., Bernasconi, M., Bethke, E., Boswell, K., Chu, D., Domokos, R. *et al.* 2015. Calibration of acoustic instruments. ICES Cooperative Research Report, 326pp.

Di Lorenzo, E., and Mantua, N. 2016. Multi-year persistence of the 2014/15 North Pacific marine heatwave. Nature Climate Change, 6: 1042–1047.

Dorman, J. G., Powell, T. M., Sydeman, W. J., and Bograd, S. J. 2011. Advection and starvation cause krill (*Euphausia pacifica*) decreases in 2005 Northern California coastal populations: implications from a model study. Geophysical Research Letters, 38: L04605.

Evans, R., English, P. A., Anderson, S. C., Gauthier, S., and Robinson, C. L. K. 2021. Factors affecting the seasonal distribution and biomass of *E . pacifica* and *T . spinifera* along the Pacific coast of Canada: a spatiotemporal modelling approach. Plos ONE, 16: e0249818.

Everson, I., Tarling, G. A., and Bergström, B. 2007. Improving acoustic estimates of krill: experience from repeat sampling of northern krill (*Meganyctiphanes norvegica*) in Gullmarsfjord, Sweden. ICES Journal of Marine Science, 64: 39–48.

Fiechter, J., Santora, J. A., Chavez, F., Northcott, D., and Messié, M. 2020. Krill hotspot formation and phenology in the California Current Ecosystem. Geophysical Research Letters, 47: e2020GL088039.

Fiedler, P. C., Reilly, S. B., Hewitt, R. P., Demer, D., Philbrick, V. A., Smith, S., Armstrong, W. *et al.* 1998. Blue whale habitat and prey in the California Channel Islands. Deep Sea Research Part II Topical Studies in Oceanography, 45: 1781–1801.

Fleischer, G. W., Cooke, K. D., Ressler, P. H., Thomas, R. E., de Blois, S. K., and Hufnagle, L. C. 2008. The 2005 integrated acoustic and trawl survey of pacific hake, *Merluccius productus*. *In* U.S. and Canadian Waters off the Pacific Coast. U.S. Department of Commerce, NOAA Technical Memorandum NMFS-NWFSC-94.: 41. U.S. Department of Commerce, Washington, DC.

Forrester, C. R., Bakkala, R. G., Okada, K., and Smith, J. E. 1983. Groundfish, shrimp, and herring fisheries in the Bering Sea and northeast Pacific–historical catch statistics, 1971-1976. International North Pacific Fisheries Commission Bulletin Number 41: 100.

Genin, A. 2004. Bio-physical coupling in the formation of zooplankton and fish aggregations over abrupt topographies. Journal of Marine Systems, 50: 3–20.

Greene, C., Wiebe, P., Pershing, A., Gal, G., Popp, J., Copley, N., Austin, T. *et al.* 1998. Assessing the distribution and abundance of zooplankton: a comparison of acoustic and net sampling methods with D-BAD MOCNESS. Deep Sea Research Part II Topical Studies in Oceanography, 45: 1219–1237.

Harris, P. T., Macmillan-Lawler, M., Rupp, J., and Baker, E. K. 2014. Geomorphology of the oceans. Marine Geology, 352: 4–24.

Harvey, C. J., Fisher, J. L., Samhouri, J. F., Williams, G. D., Francis, T. B., Jacobson, K. C., deReynier, Y. L. *et al.* 2020. The importance of long-term ecological time series for integrated ecosystem assessment and ecosystem-based management. Progress in Oceanography, 188: 102418.

Hewitt, R. P., Demer, D. A., and Emery, J. H. 2003. An 8-year cycle in krill biomass density inferred from acoustic surveys conducted in the vicinity of the South Shetland Islands during the austral summers of 1991–1992 through 2001–2002. Aquatic Living Resources, 16: 205–213.

Jacox, M. G., Alexander, M. A., Mantua, N. J., Scott, J. D., Hervieux, G., Webb, R. S., and Werner, F. E. 2018. Forcing of multiyear extreme

ocean temperatures that impacted California Current living marine resources in 2016. Bulletin of the American Meteorological Society, 99: S27–S33.

Jones, T., Parrish, J. K., Peterson, W. T., Bjorkstedt, E. P., Bond, N. A., Ballance, L. T., Bowes, V. *et al.* 2018. Massive mortality of a planktivorous seabird in response to a marine heatwave. Geophysical Research Letters, 45: 3193–3202. doi: 10.1002/2017GL076164.

Lavaniegos, B. E., Jiménez-Herrera, M., and Ambriz-Arreola, I. 2019. Unusually low euphausiid biomass during the warm years of 2014–2016 in the transition zone of the California Current. Deep Sea Research Part II Topical Studies in Oceanography, 169-170: 104638.

Leising, A. W., Schroeder, I. D., Bograd, S. J., Abell, J., Durazo, R., Gaxiola-Castro, G., Bjorkstedt, E. P. *et al.* 2015. State of the California Current 2014–15: impacts of the warm-water "Blob". CalCOFI Report, 56: 31–68.

Livingston, P. A. 1983. Food habits of Pacific whiting, *Merluccius productus*, off the west coast of North America, 1967 and 1980. Fishery Bulletin, 81: 629–636.

McClatchie, S., Thorne, R. E., Grimes, P., and Hanchet, S. 2000. Ground truth and target identification for fisheries acoustics. Fisheries Research, 47: 173–191.

McHenry, J., Welch, H., Lester, S. E., and Saba, V. 2019. Projecting marine species range shifts from only temperature can mask climate vulnerability. Global Change Biology, 25: 4208–4221.

McKelvey, D. R., and Wilson, C. D. 2006. Discriminant classification of fish and zooplankton backscattering at 38 and 120 kHz. Transactions of the American Fisheries Society, 135: 488–499.

McQuinn, I. H., Plourde, S., Pierre, St., and Dion, M. 2015. Spatial and temporal variations in the abundance, distribution, and aggregation of krill (*Thysanoessa raschii* and *Meganyctiphanes norvegica*) in the lower estuary and Gulf of St. Lawrence. Progress in Oceanography, 131: 159–176.

Mackas, D. L. 1992. Seasonal cycle of zooplankton off southwestern British Columbia: 1979–89. Canadian Journal of Fisheries and Aquatic Sciences, 49: 903–921.

Mackas, D. L., Denman, K. L., and Abbott, M. R. 1985. Plankton patchiness: biology in the physical vernacular. Bulletin of Marine Science, 37: 652–674.

Mackas, D. L., Kieser, R., Saunders, M., Yelland, D. R., Brown, R. M., and Moore, D. F. 1997. Aggregation of euphausiids and pacific hake (*Merluccius productus*) along the outer continental shelf off Vancouver Island. Canadian Journal of Fisheries and Aquatic Sciences, 54: 2080–2096.

Mackas, D. L., Thomson, R. E., and Galbraith, M. 2001. Changes in the zooplankton community of the British Columbia continental margin, 1985-1999, and their covariation with oceanographic conditions. Canadian Journal of Fisheries and Aquatic Sciences, 58: 685–702.

Malick, M. J., Cox, S. P., Mueter, F. J., Dorner, B., and Peterman, R. M. 2017. Effects of the North Pacific Current on the productivity of 163 Pacific salmon stocks. Fisheries Oceanography, 26: 268–281.

Malick, M. J., Hunsicker, M. E., Haltuch, M. A., Parker-Stetter, S. L., Berger, A. M., and Marshall, K. N. 2020. Relationships between temperature and pacific hake distribution vary across latitude and life-history stage. Marine Ecology Progress Series, 639: 185–197.

Marinovic, B. B., Croll, D. A., Gong, N., Benson, S. R., and Chavez, F. P. 2002. Effects of the 1997–1999 El Niño and La Niña events on zooplankton abundance and euphausiid community composition within the Monterey Bay coastal upwelling system. Progress in Oceanography, 54: 265–277.

Mauchline, J., and Fisher, L. R. 1969. The biology of euphausiids. *In* Advances in Marine Biology, Ed. by F. S. Russell, and M. Yonge. Academic Press, Cambridge, MA. http://www.sciencedirect.com/science/article/pii/S006528810860468X.

Mendelssohn, R. 2020. rerddapXtracto: extracts environmental data from 'ERDDAP' web services. https://CRAN.R-project.org/package=rerddapXtracto (last accessed 9 July 2020).

Miyashita, K., Aoki, I., and Inagaki, T. 1996. Swimming behaviour and target strength of isada krill (*Euphausia pacifica*). ICES Journal of Marine Science, 53: 303–308.

NASA/GSFC OBPG. 2020. MODIS-Aqua level-3 mapped chlorophyll data version 2018. https://oceancolor.gsfc.nasa.gov/data/10.5067/AQUA/MODIS/L3M/CHL/2018 (last accessed 10 July 2020).

National Geophysical Data Center. 2003. U.S. Coastal Relief Model Vol.8 - Northwest Pacific. National Geophysical Data Center, NOAA. https://data.nodc.noaa.gov/cgi-bin/iso?id=gov.noaa.ngdc.mgg.dem:288# (last accessed 29 April 2020).

National Geophysical Data Center. 2013. British Columbia 3 arc-second bathymetric digital elevation model. National Geophysical Data Center, NOAA. https://www.ngdc.noaa.gov/metaview/page?xml=NOAA/NESDIS/NGDC/MGG/DEM/iso/xml/4956.xml&view=getDataView&header=none (last accessed 29 April 2020).

Neveu, E., Moore, A. M., Edwards, C. A., Fiechter, J., Drake, P., Crawford, W. J., Jacox, M. G. *et al.* 2016. An historical analysis of the California Current circulation using ROMS 4D-Var: system configuration and diagnostics. Ocean Modelling, 99: 133–151.

Pedersen, E. J., Miller, D. L., Simpson, G. L., and Ross, N. 2019. Hierarchical generalized additive models in ecology: an introduction with mgcv. PeerJ, 7: e6876.

Peterson, W. T., Brodeur, R. D., and Pearcy, W. G. 1982. Food habits of juvenile salmon in the Oregon coastal zone, June 1979. Fishery Bulletin, 80: 841–851.

Peterson, W. T., Feinberg, L., and Keister, J. E. 2000. Ecological zonation of euphausiids off central Oregon. *In* Workshop of the PICES-GLOBEC International Program on Climate Change and Carrying Capacity. pp. 125–128. North Pacific Marine Science Organization, Sidney, BC.

Peterson, W. T., Fisher, J. L., Strub, P. T., Du, X., Risien, C., Peterson, J., and Shaw, C. T. 2017. The pelagic ecosystem in the Northern California Current off Oregon during the 2014–2016 warm anomalies within the context of the past 20 years. Journal of Geophysical Research Oceans, 122: 7267–7290.

R Core Team. 2016. R: A Language and Evironment for Statistical Computing. R Foundation for Statistical Computing, Vienna. http://www.R-project.org/ (last accessed: February 20, 2022).

Ressler, P. H., Brodeur, R. D., Peterson, W. T., Pierce, S. D., Mitchell Vance, P., Røstad, A., and Barth, J. A. 2005. The spatial distribution of euphausiid aggregations in the Northern California Current during August 2000. Deep Sea Research Part II Topical Studies in Oceanography, 52: 89–108.

Richardson, A. J. 2008. In hot water: zooplankton and climate change. ICES Journal of Marine Science, 65: 279–295.

Robertson, R. R., and Bjorkstedt, E. P. 2020. Climate-driven variability in *Euphausia pacifica* size distributions off northern California. Progress in Oceanography, 188: 102412.

Sandwell, D. T., Becker, J. J., Olson, C., and Jackson, A. 2014. SRTM15_PLUS: Data fusion of Shuttle Radar Topography Mission (SRTM) land topography with measured and estimated seafloor topography (NCEI Accession 0150537) - Data.gov. Scripps Institution of Oceanography - University of California, San Diego, CA. https://catalog.data.gov/dataset/srtm15-plus-data-fusion-of-shuttle-radar-topography-mission-srtm-land-topography-with-measured- (last accessed 29 April 2020).

Santora, J. A., Sydeman, W. J., Schroeder, I. D., Wells, B. K., and Field, J. C. 2011. Mesoscale structure and oceanographic determinants of krill hotspots in the California Current: implications for trophic transfer and conservation. Progress in Oceanography, 91: 397–409.

Santora, J. A., Zeno, R., Dorman, J. G., and Sydeman, W. J. 2018. Submarine canyons represent an essential habitat network for krill hotspots in a large marine ecosystem. Scientific Reports, 8: 7579.

Simons, R. A. 2019. ERDDAP. https://coastwatch.pfeg.noaa.gov/erddap (last accessed 10 July 2020).

Simonsen, K. A., Ressler, P. H., Rooper, C. N., and Zador, S. G. 2016. Spatio-temporal distribution of euphausiids: an important

component to understanding ecosystem processes in the Gulf of Alaska and eastern Bering Sea. ICES Journal of Marine Science, 73: 2020–2036.

Skjoldal, H. R., Wiebe, P., Postel, L., Knutsen, T., Kaartvedt, S., and Sameoto, D. 2013. Intercomparison of zooplankton (net) sampling systems: results from the ICES/GLOBEC sea-going workshop. Progress in Oceanography, 108: 1–42.

Smith, W. H. F., and Sandwell, D. T. 1997. Global sea floor topography from satellite altimetry and ship depth soundings. Science, 277: 1956–1962.

Swartzman, G., and Hickey, B. 2003. Evidence for a regime shift after the 1997-1998 El Niño, based on 1995, 1998, and 2001 acoustic surveys in the Pacific eastern boundary current. Estuaries, 26: 1032–1043.

Sydeman, W. J., Bradley, R. W., Warzybok, P., Abraham, C. L., Jahncke, J., Hyrenbach, K. D., and Kousky, V. 2006. Planktivorous auklet *Ptychoramphus aleuticus* responses to ocean climate, 2005: unusual atmospheric blocking?. Geophysical Research Letters, 33: 42113015.

Sydeman, W. J., Santora, J. A., Thompson, S. A., Marinovic, B., and Lorenzo, E. D. 2013. Increasing variance in North Pacific climate relates to unprecedented ecosystem variability off California. Global Change Biology, 19: 1662–1675.

Sydeman, W. J., Thompson, S. A., Field, J. C., Peterson, W. T., Tanasichuk, Freeland, H., J., and Bograd, S. J. 2011. Does positioning of the North Pacific Current affect downstream ecosystem productivity?. Geophysical Research Letters, 38: 129562519.

Wood, S. N. 2006. Generalized Additive Models: An Introduction with R. Chapman and Hall/CRC, Boca Raton, FL. 410pp.

Wood, S. N., and Augustin, N. H. 2002. GAMs with integrated model selection using penalized regression splines and applications to environmental modelling. Ecological Modelling, 157: 157–177.

Worton, B. J. 1989. Kernel methods for estimating the utilization distribution in home-range studies. Ecology, 70: 164–168.

Zar, J. H. 1999. Biostatistical Analysis. Prentice Hall, Upper Saddle River, NJ.

Handling Editor: Olav Rune Godo